

Transfer learning from Hermitian to non-Hermitian quantum many-body physics

Sharareh Sayyad^{1,*} and Jose L. Lado²

¹Max Planck Institute for the Science of Light, Staudtstraße 2, 91058 Erlangen, Germany

²Department of Applied Physics, Aalto University, FI-00076 Aalto, Espoo, Finland

Identifying phase boundaries of interacting systems is one of the key steps to understanding quantum many-body models. The development of various numerical and analytical methods has allowed exploring the phase diagrams of many Hermitian interacting systems. However, numerical challenges and scarcity of analytical solutions hinder obtaining phase boundaries in non-Hermitian many-body models. Recent machine learning methods have emerged as a potential strategy to learn phase boundaries from various observables without having access to the full many-body wavefunction. Here, we show that a machine learning methodology trained solely on Hermitian correlation functions allows identifying phase boundaries of non-Hermitian interacting models. These results demonstrate that Hermitian machine learning algorithms can be redeployed to non-Hermitian models without requiring further training to reveal non-Hermitian phase diagrams. Our findings establish transfer learning as a versatile strategy to leverage Hermitian physics to machine learning non-Hermitian phenomena.

Introduction. The interplay between various degrees of freedom in many-body systems results in the emergence of novel phases of matter, including superconducting [1–6], Mott insulating [7–11], nematic [12–16] and topological [17–22] phases. Due to their inherent complexity, these systems are often studied computationally, using, e.g., quantum Monte Carlo methods [23–25] and tensor network approaches [26–28]. In recent years, machine learning methods [29, 30] have provided a complementary strategy to rationalize phases of matter, often in combination with conventional quantum many-body methods. The demonstrations of these roles played by machine learning methods in tackling many-body problems results in characterizing different phases of matter [31–40], deep learning of the quantum dynamics [41–44], obtaining many-body wave functions [45–49], and optimizing the performance of computational simulations [50].

Exploring correlated physics in open quantum systems attracts great interest mainly because of the systematic treatment of loss and gain in these systems, which quantitatively reproduces experimental observations [51–55]. In recent years, along with brute force studies of open quantum systems, understanding their effective descriptions based on non-Hermitian physics get momentum [56–61]. The studies of non-Hermitian models have initially focused on single-particle models [62–78], and its extension to the fully interacting realm has also gained attention recently [79–95]. Aside from these case studies, unraveling the physics of interacting non-Hermitian systems remains an open challenge due to the scarcity of exactly solvable models, and as conventional (Hermitian) many-body methods cannot be directly applied to the non-Hermitian limit. Specifically, obtaining the phase boundaries, understanding the stability of certain phases against non-Hermiticity, and characterizing exotic phases with no Hermitian counterparts remain in general open problems. Similar to the realm of Hermitian physics, ma-

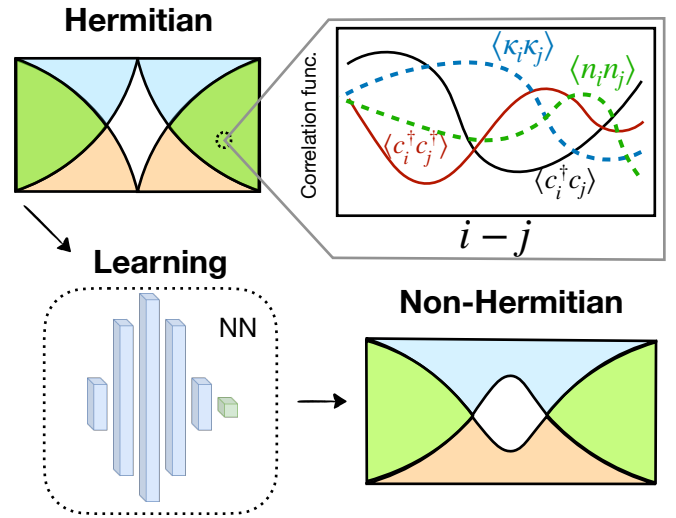


Figure 1. **Non-Hermitian transfer learning:** Schematic illustration of the transfer learning methodology from Hermitian models to non-Hermitian physics. As an input, for each point of the phase diagram of the Hermitian model, short-range two-point (solid lines) and four-point (dashed lines) correlation functions are computed (Eqs.(4) and (5)). The generated correlators for Hermitian systems are used to train a machine learning architecture, which in turn allows predicting the phase diagram from short-range correlators of the non-Hermitian model. The machine learning methodology allows extracting quasi-degeneracies and correlation entropies from the short-range correlators of the non-Hermitian model.

chine learning methods, and specifically supervised [96–99], unsupervised [99, 100], and graph-informed methods [101] allowed to identify various phases of non-Hermitian non-interacting systems. In these methodologies, the inputs to train learning models are collected from non-Hermitian noninteracting systems and are used to characterize non-Hermitian phase diagrams. As computational methods for Hermitian interacting models are numerically less demanding and more stable than their

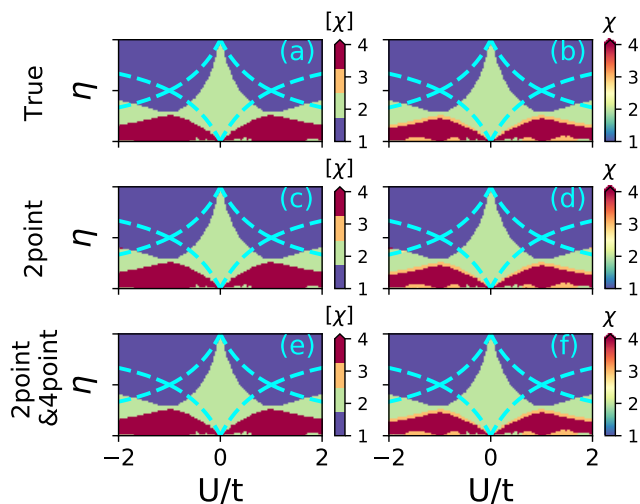


Figure 2. **Hermitian interacting model:** The phase diagram of the Hermitian many-body model with $L = 16$ on the $U/t - \eta$ plane at $\delta = 0.0$. The results in (a) and (b) are calculated by exact diagonalization. Panels (c,d) use a machine learning architecture that uses solely two-point correlation functions as input. In contrast, panels (e,f) use an architecture trained on both two-point and four-point correlation functions. The quasi-degeneracy in (c,e) is treated as a discrete classifier for $[\chi]$, while it is treated as a regression problem in (d,f). The boundaries in the thermodynamic limit are shown by cyan dashed lines.

non-Hermitian counterparts, learning phase diagrams of non-Hermitian many-body systems from Hermitian correlated models would open up a promising strategy to leverage many-body methods developed for interacting Hermitian models.

In this manuscript, we show that machine learning methods purely trained on Hermitian many-body data can predict interacting regimes in non-Hermitian interacting models. For concreteness purposes, we explore the different regimes of the non-Hermitian dimerized Kitaev-Hubbard chain using machine learning techniques schematically shown in Fig. 1. Here, we collect various correlation functions, orders of quasi-degeneracies, and correlation entropies at different parameter regimes of the Hermitian limit of our model. Using this input, we demonstrate that non-Hermitian regime crossovers can be identified using a machine-learning methodology trained on short-range Hermitian correlation functions. The outcomes of these supervised learning schemes are degrees of quasi-degeneracies and correlation entropies, which can characterize various regimes of the non-Hermitian model. Our findings reveal that employing correlation entropy as a classifier allows characterizing all regimes of the system. Our machine-learning approach reliably learns various regimes that share similarities with the Hermitian model. Our method also successfully delineates the regime crossovers even when the

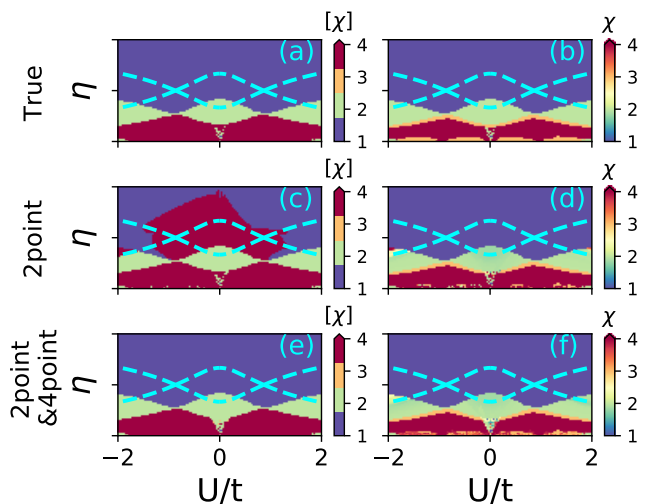


Figure 3. **Non-Hermitian interacting model:** The regimes of the non-Hermitian many-body model with $L = 16$ on the $U/t - \eta$ plane at $\delta = 0.5$. The results in (a) and (b) are calculated by exact diagonalization. The regimes in (c,d) are obtained using architectures trained by two-point correlations, whereas (e,f) are trained on both two-point and four-point correlation functions. The quasi-degeneracy in (c,e) is treated as a discrete classifier for $[\chi]$, while it is treated as a regression problem in (d,f). The boundaries in the thermodynamic limit are shown by cyan dashed lines and black dashed-dotted lines. It is observed that while two-point correlators fail to predict the non-Hermitian regimes in (c), the inclusion of four-point correlators recovers accurate regime crossovers (e).

correlation effect in the non-Hermitian interacting model deforms the Hermitian phase diagram.

Non-Hermitian interacting model. We focus on an interacting non-Hermitian model whose phase boundaries can be solved exactly in the thermodynamic limit [91]. The non-Hermitian dimerized Kitaev-Hubbard Hamiltonian on a chain with length L is given by

$$\mathcal{H} = - \sum_{j=1}^{L-1} \left[t_j \left(c_j^\dagger c_{j+1} + c_{j+1}^\dagger c_j \right) + \Delta_j \left(c_j^\dagger c_{j+1}^\dagger + c_{j+1} c_j \right) \right] + \sum_{j=1}^{L-1} (U_j - i\delta_j) (2n_j - 1) (2n_{j+1} - 1), \quad (1)$$

where c_j^\dagger (c_j) is a creation (annihilation) operator for spinless fermion at site j associated with the fermion density $n_j = c_j^\dagger c_j$. Here t_j , Δ_j , and $U_j - i\delta_j$ denote, respectively, real-valued dimerized hopping amplitude, superconducting pairing amplitude, and complex-valued Hubbard interaction strength. Considering the site-independent parameter $\mathcal{O} \in \{t, \Delta, U, \delta\}$, $\mathcal{O}_j \in \{t_j, \Delta_j, U_j, \delta_j\}$ for $1 \leq j \leq L$ reads $\mathcal{O}_j = \mathcal{O}(1 - \eta)$ if $j \bmod 2 = 0$ and $\mathcal{O}_j = \mathcal{O}(1 + \eta)$ if $j \bmod 2 = 1$, where η is the real-valued dimerization parameter.

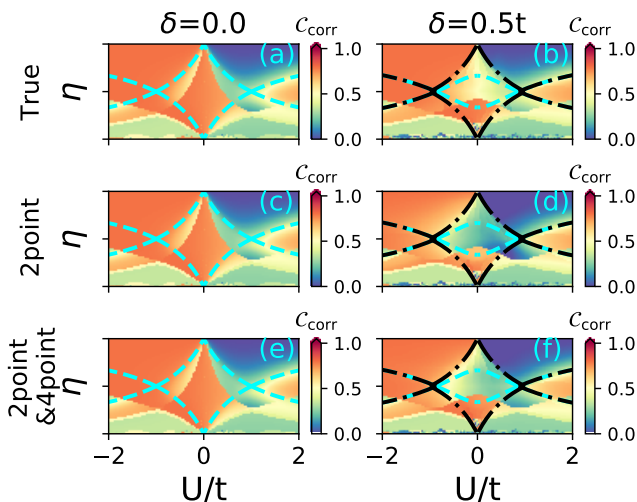


Figure 4. **Correlation entropy predictions:** The regimes of the non-Hermitian many-body model with $L = 16$ on the $U/t - \eta$ plane at $\delta = 0.0$ (a,c,e), $0.5t$ (b,d,f). The trained models are obtained using the Hermitian datasets with $\delta = 0.0$. The color bar denotes C_{corr} . The regimes panels (c,d) are obtained using the machine learning model trained by two-point correlation functions, whereas (e,f) are trained on both two-point and four-point correlation functions. The boundaries in the thermodynamic limit given in the main text are shown by cyan dashed lines and black dashed-dotted lines.

The Hamiltonian in Eq. (1) is exactly solvable when $\Delta = t$. At this parameter regime, the interacting model can be mapped to a quadratic fermionic model upon successive two Jordan-Wigner transformations and a spin rotation [91]. Through this procedure, one can show that the spectrum of the effective quadratic Hamiltonian undergoes gap closure upon setting $\frac{U}{t} = \pm \sqrt{\frac{\delta^2}{t^2} - \frac{(1 \pm \eta)^2}{(1 \mp \eta)^2}}$, and $\frac{U}{t} = \pm \frac{1 \pm \eta}{1 \mp \eta}$. These relations ensure the closure of the real-line gaps and the appearance of zero degeneracies in the imaginary part of the spectrum, respectively. Note that these two equations coincide when the non-Hermiticity parameter vanishes, i.e., $\delta = 0$.

As \mathcal{H} respects the charge conjugation symmetry, eigenvalues come in pairs such that the set of all energies satisfy $\{\varepsilon\} = \{\varepsilon^*\}$. This implies that degeneracies of phases can be merely obtained by vanishing real parts of the spectrum. In a finite system, finite size effects will give rise to small splitting between degenerate states in the thermodynamic limit. For finite models, it is thus convenient to define the quasi-degeneracy χ given by

$$\chi = \sum_{\alpha} e^{-\lambda|\varepsilon_{\alpha} - \varepsilon_0|} \quad (2)$$

with ε_{α} being the α th eigenvalue, and ε_0 the ground state [102]. The parameter λ controls the energy resolution of the quasi-degeneracy, which in the limiting case $\lim_{\lambda \rightarrow \infty} \lim_{L \rightarrow \infty} \chi$ becomes the thermodynamic degeneracy

of the ground state [103]. We will focus our analysis on system sizes with $L = 16$, that are large enough to show different transition regimes that would converge to the different phases of the model in the thermodynamic limit.

In addition to the quasi-degeneracy χ , we can characterize the phase boundaries using the electronic correlation entropy given by [34, 104–107]

$$C_{\text{corr}} = -\frac{1}{L} \sum_{j=1}^L s_j \log(s_j), \quad (3)$$

where $0 \leq s_j \leq 1$ is the j th eigenvalue of the correlation matrix. The elements of the correlation matrix C^{mat} are two-point correlation functions that read $C_{ij}^{\text{mat}} = |\det[\sum_{l'l''}^{[\chi]} \rho_{ij}^{l'l''}]|$ with $\rho_{ij}^{l'l''} = \langle \Psi_l | c_i^{\dagger} c_j | \Psi_{l''} \rangle$, where Ψ_l is the l th eigenstate on the ground state manifold, and $[\chi]$ is the closest integer to χ . The correlation matrix C_{corr} measures many-body entanglement and vanishes in systems described by Hartree-Fock product states [34, 108–111]. It is worth noting that while superconducting states can be represented as a product state in the Nambu basis, the previous definition of correlation entropy yields a finite value for superconducting states. Large values of C_{corr} in certain regions of the phase diagram imply that the system cannot be represented by a Hartree-Fock product state.

Machine learning methodology. We now present the machine learning methodology to learn the different regimes of the interacting models, taking as target functions χ and C_{corr} . The input of our machine-learning algorithm corresponds to short-range many-body correlators in the form of two-point and four-point correlation functions given by

$$d_{ij} = \langle c_i^{\dagger} c_j \rangle_{[\chi]}, \quad f_{ij} = \langle c_i^{\dagger} c_j^{\dagger} \rangle_{[\chi]}, \quad (4)$$

$$k_{ij} = \langle \kappa_{ij} \kappa_{ij}^{\dagger} \rangle_{[\chi]}, \quad p_{ij} = \langle n_i n_j \rangle_{[\chi]}, \quad (5)$$

where $\kappa_{ij} = c_i c_j$ and $\langle \hat{A} \rangle_{[\chi]} \equiv |\det[\sum_{l'l''}^{[\chi]} A_{ll'']}]|$ with $A_{ll''} = \langle \Psi_l | \hat{A} | \Psi_{l''} \rangle$. Here, i, j run on four neighboring sites in the middle of the chain so that the algorithm relies solely on short-range correlation functions. These correlation functions are used to predict the quasi-degeneracy χ and the correlation entropy C_{corr} . We collect 20000 different non-Hermitian interacting realizations on the $(U/t, \eta)$ plane, taking the non-Hermiticity parameter as $\delta \in \{0, 0.5\}$. To predict the quasi-degeneracy, we explore two strategies, the first one is based on transforming the task in a classification problem for $[\chi]$, and the second one is a regression problem for χ . The prediction of C_{corr} is treated as a regression problem. The details of our NN architecture for each of these cases are presented in the Supplemental Materials (SM) [112].

Results. We now present the predictions of different regimes based on various correlators for our Hermitian

and non-Hermitian limits. We start with the Hermitian phase diagram shown in Fig. 2 (a,b). These panels present the numerical regimes obtained with the exact diagonalization method [113]. The finite-size effect pushed the regime crossovers to smaller η values from the phase boundaries in the thermodynamic limit, a feature that can be systematically analyzed using finite size scaling [91]. Performing this scaling gives rise to the thermodynamic phase boundaries shown in the cyan lines [91].

The associated predicted regime crossovers using χ are displayed in Fig. 2 (c,d,e,f). Here, we compare the true (Fig. 2ab) and predicted (Fig. 2(c,d,e,f)) phase diagrams obtained from training the NN model using the two-point correlation functions (Fig. 2(c,d)) or the combination of both two-point and four-point correlation functions (Fig. 2(e,f)). The values of $[\chi]$ in Fig. 2(a,c,e) are discrete, and the predicted results belong to different classes of $[\chi]$. In panels Fig. 2(b,d,f), a regression architecture is used to predict χ , and the predicted results Fig. 2(d,f) are obtained as a regression problem.

We now examine how the regimes of the non-Hermitian interacting model can be deduced from short-range correlators using a model trained by the Hermitian dataset with $\delta = 0.0$, as shown in Fig. 3. Fig. 3(c,d,e,f) shows the predicted phase crossovers obtained by the algorithm trained with Hermitian data, which should be compared with true outputs of the non-Hermitian problem shown in Fig. 3(a,b). Interestingly, the predicted results based on two-point correlation functions based on a classification architecture for $[\chi]$ (Fig. 3(c)) display a large discrepancy. Such inaccurate prediction is eliminated by incorporating four-point correlation functions into the considered observables, as shown in Fig. 3(e). We further note that if we phrase the task as a regression problem, as shown in Fig. 3(b,d,f), the predicted phase boundaries based on training with two-point correlation functions are more reliable, as shown in Fig. 3(d). These results show that the quasidegeneracy of the non-Hermitian model can be extracted from a model trained purely on Hermitian data.

Aside from χ , the different regimes can be characterized using the correlation entropy $\mathcal{C}_{\text{corr}}$ both in Hermitian $\delta = 0$ and non-Hermitian $\delta = 0.5t$ systems as respectively shown in Fig. 4 (a,b). Finite-size effects are reflected in the deviations from the cyan lines, which are inherited by the changes of $[\chi]$ that impact the definition of the correlation entropy. Interestingly, $\mathcal{C}_{\text{corr}}$ exhibits further transitions, quantitatively described by the analytic phase boundaries. The absence of a finite size effect in different regions of the parameter space, delineated by the black dashed-dotted lines, signals the exponential convergence towards the ground state due to finite correlation gaps. Similar behavior is reported in Mott insulators [34, 114] and magnetic vortex liquids [115]. In Fig. 4, we present the various regimes for Hermitian (Fig. 4(a,c,e)) and non-Hermitian (Fig. 4(b,d,f)) systems using a model trained on Hermitian models with only two-point (Fig. 4(c,d)) or

the combination of two-point and four-point correlation functions (Fig. 4(e,f)). Overall, all the thermodynamic phase boundaries are qualitatively signaled by the correlation entropy. In the non-Hermitian cases, we can identify some regions, mainly inside the black diamond-like phase boundaries, featuring differences from the true results. These differences are reduced when including four-point correlation functions in the training of the Hermitian model; see also the SM [112]. It is worth noting that the regions with the most discrepancies have a topological superconducting nature, suggesting that phases with topological and many-body effects require higher-point correlation functions to be inferred with short-range information.

Our machine learning models trained only in Hermitian Hamiltonians can characterize the regimes of non-Hermitian interacting systems. It is interesting to note that, while we observe a general agreement, small discrepancies between the machine learning predicted regimes and the computationally exact ones can be observed. This is because non-Hermitian many-body systems can show richer ground states than their Hermitian analog due to the extent of their spectrum in the complex plane. As a result, many-body wavefunctions in non-Hermitian models are genuinely different from their Hermitian counterparts, as these wavefunctions can span different regions of the Hilbert space beyond the original Hermitian training. Interestingly, this discrepancy opens the possibility of using our machine learning algorithms to directly identify non-Hermitian phases that do not have a Hermitian counterpart.

Conclusion. To summarize, we have demonstrated a transfer machine learning methodology whereby training on Hermitian many-body models allows us to predict different regimes of interacting non-Hermitian quantum many-body models. This opens the possibility of employing Hermitian many-body physics to understand the phase boundaries of non-Hermitian systems, leveraging solutions and methodologies currently only applicable to quantum many-body models. Our findings reveal that the prediction of quasi-degeneracy or correlation entropy allows the identification of different regions in interacting systems. Interestingly, these two methodologies are affected in a qualitatively different manner for finite size effects, with the correlation entropy showing the fastest convergence to the thermodynamic limit. Our machine-learning methodology relies on short-range correlation functions, which open the possibility to potential deployments of our technique in experimental setups. Our results establish transfer learning as a promising strategy to map regimes on non-Hermitian quantum many-body models and to identify regimes featuring phenomena not observable in Hermitian models.

Acknowledgements: S.S. thanks F. Marquardt for the helpful discussions. J.L.L. acknowledges the computational resources provided by the Aalto Science-IT

project, the financial support from the Academy of Finland Projects No. 331342, No. 336243 and No 349696, and the Jane and Aatos Erkko Foundation.

* sharareh.sayyad@mpl.mpg.de

- [1] JMB Lopes Dos Santos, NMR Peres, and AH Castro Neto, “Graphene bilayer with a twist: Electronic structure,” *Physical review letters* **99**, 256802 (2007).
- [2] Cyril Proust and Louis Taillefer, “The remarkable underlying ground states of cuprate superconductors,” *Annual Review of Condensed Matter Physics* **10**, 409–429 (2019).
- [3] Eva Y Andrei and Allan H MacDonald, “Graphene bilayers with a twist,” *Nature materials* **19**, 1265–1275 (2020).
- [4] Sharareh Sayyad, Edwin W. Huang, Motoharu Kitatani, Mohammad-Sadegh Vaezi, Zohar Nussinov, Abolhassan Vaezi, and Hideo Aoki, “Pairing and non-fermi liquid behavior in partially flat-band systems: Beyond nesting physics,” *Phys. Rev. B* **101**, 014501 (2020).
- [5] Yusuke Nomura and Ryotaro Arita, “Superconductivity in infinite-layer nickelates,” *Reports on Progress in Physics* **85**, 052501 (2022).
- [6] Motoharu Kitatani, Liang Si, Paul Worm, Jan M. Tomczak, Ryotaro Arita, and Karsten Held, “Optimizing superconductivity: From cuprates via nickelates to palladates,” *Phys. Rev. Lett.* **130**, 166002 (2023).
- [7] Sharareh Sayyad and Martin Eckstein, “Slowdown of the electronic relaxation close to the mott transition,” *Phys. Rev. Lett.* **117**, 096403 (2016).
- [8] Kangjun Seo, Valeri N Kotov, and Bruno Uchoa, “Ferromagnetic mott state in twisted graphene bilayers at the magic angle,” *Physical review letters* **122**, 246402 (2019).
- [9] Maria Chatzieftheriou, Alexander Kowalski, Maja Berović, Adriano Amaricci, Massimo Capone, Lorenzo De Leo, Giorgio Sangiovanni, and Luca De’Medici, “Mott quantum critical points at finite doping,” *Physical Review Letters* **130**, 066401 (2023).
- [10] Sunghoon Kim, T Senthil, and Debanjan Chowdhury, “Continuous mott transition in moiré semiconductors: role of long-wavelength inhomogeneities,” *Physical Review Letters* **130**, 066301 (2023).
- [11] Yu-Chin Tzeng, Po-Yao Chang, and Min-Fong Yang, “Interaction-induced metal to topological insulator transition,” *Physical Review B* **107**, 155106 (2023).
- [12] RM Fernandes, AV Chubukov, and J Schmalian, “What drives nematic order in iron-based superconductors?” *Nature physics* **10**, 97–104 (2014).
- [13] Rhine Samajdar, Mathias S Scheurer, Simon Turkel, Carmen Rubio-Verdú, Abhay N Pasupathy, Jörn W F Venderbos, and Rafael M Fernandes, “Electric-field-tunable electronic nematic order in twisted double-bilayer graphene,” *2D Materials* **8**, 034005 (2021).
- [14] Sharareh Sayyad, Motoharu Kitatani, Abolhassan Vaezi, and Hideo Aoki, “Nematicity-enhanced superconductivity in systems with a non-fermi liquid behavior,” *Journal of Physics: Condensed Matter* **35**, 245605 (2023).
- [15] Kiyotaka Mukasa, Kousuke Ishida, Shusaku Imajo, Mingwei Qiu, Mikihiro Saito, Kohei Matsuura, Yuichi Sugimura, Supeng Liu, Yu Uezono, Takumi Otsuka, *et al.*, “Enhanced superconducting pairing strength near a pure nematic quantum critical point,” *Physical Review X* **13**, 011032 (2023).
- [16] Qianni Jiang, Yue Shi, Morten H Christensen, Joshua J Sanchez, Bevin Huang, Zhong Lin, Zhaoyu Liu, Paul Malinowski, Xiaodong Xu, Rafael M Fernandes, *et al.*, “Nematic fluctuations in an orbital selective superconductor $\text{Fe}_{1+y}\text{Te}_{1-x}\text{Se}_x$,” *Communications Physics* **6**, 39 (2023).
- [17] DN Sheng, Zheng-Cheng Gu, Kai Sun, and L Sheng, “Fractional quantum hall effect in the absence of landau levels,” *Nature communications* **2**, 389 (2011).
- [18] Titus Neupert, Luiz Santos, Claudio Chamon, and Christopher Mudry, “Fractional quantum hall states at zero magnetic field,” *Physical review letters* **106**, 236804 (2011).
- [19] Frank Pollmann, Erez Berg, Ari M. Turner, and Masaki Oshikawa, “Symmetry protection of topological phases in one-dimensional quantum spin systems,” *Phys. Rev. B* **85**, 075125 (2012).
- [20] Bela Bauer and Chetan Nayak, “Area laws in a many-body localized state and its implications for topological order,” *Journal of Statistical Mechanics: Theory and Experiment* **2013**, P09005 (2013).
- [21] Frederick del Pozo, Loic Herviou, and Karyn Le Hur, “Fractional topology in interacting one-dimensional superconductors,” *Physical Review B* **107**, 155134 (2023).
- [22] Sunghoon Kim, Adhip Agarwala, and Debanjan Chowdhury, “Fractionalization and topology in amorphous electronic solids,” *Physical Review Letters* **130**, 026202 (2023).
- [23] Matthias Troyer and Uwe-Jens Wiese, “Computational complexity and fundamental limitations to fermionic quantum monte carlo simulations,” *Phys. Rev. Lett.* **94**, 170201 (2005).
- [24] A. Gezerlis, I. Tews, E. Epelbaum, S. Gandolfi, K. Hebeler, A. Nogga, and A. Schwenk, “Quantum monte carlo calculations with chiral effective field theory interactions,” *Phys. Rev. Lett.* **111**, 032501 (2013).
- [25] Mohammad-Sadegh Vaezi, Amir-Reza Negari, Amin Moharramipour, and Abolhassan Vaezi, “Amelioration for the sign problem: An adiabatic quantum monte carlo algorithm,” *Phys. Rev. Lett.* **127**, 217003 (2021).
- [26] Román Orús, “A practical introduction to tensor networks: Matrix product states and projected entangled pair states,” *Annals of Physics* **349**, 117–158 (2014).
- [27] Román Orús, “Tensor networks for complex quantum systems,” *Nature Reviews Physics* **1**, 538–550 (2019).
- [28] J. Ignacio Cirac, David Perez-Garcia, Norbert Schuch, and Frank Verstraete, “Matrix product states and projected entangled pair states: Concepts, symmetries, theorems,” *Rev. Mod. Phys.* **93**, 045003 (2021).
- [29] Pankaj Mehta, Marin Bukov, Ching-Hao Wang, Alexandre G.R. Day, Clint Richardson, Charles K. Fisher, and David J. Schwab, “A high-bias, low-variance introduction to machine learning for physicists,” *Physics Reports* **810**, 1–124 (2019), a high-bias, low-variance introduction to Machine Learning for physicists.
- [30] Giuseppe Carleo, Ignacio Cirac, Kyle Cranmer, Laurent Daudet, Maria Schuld, Naftali Tishby, Leslie Vogt-Maranto, and Lenka Zdeborová, “Machine learning

- and the physical sciences,” *Rev. Mod. Phys.* **91**, 045002 (2019).
- [31] Peter Broecker, Juan Carrasquilla, Roger G Melko, and Simon Trebst, “Machine learning quantum phases of matter beyond the fermion sign problem,” *Scientific reports* **7**, 1–10 (2017).
- [32] Joaquin F Rodriguez-Nieva and Mathias S Scheurer, “Identifying topological order through unsupervised machine learning,” *Nature Physics* **15**, 790–795 (2019).
- [33] Mathias S Scheurer and Robert-Jan Slager, “Unsupervised machine learning and band topology,” *Physical review letters* **124**, 226401 (2020).
- [34] Faluke Aikebaier, Teemu Ojanen, and Jose L. Lado, “Extracting electronic many-body correlations from local measurements with artificial neural networks,” *SciPost Phys. Core* **6**, 030 (2023).
- [35] Evert P. L. van Nieuwenburg, Ye-Hua Liu, and Sebastian D. Huber, “Learning phase transitions by confusion,” *Nature Physics* **13**, 435–439 (2017).
- [36] Rouven Koch and Jose L. Lado, “Designing quantum many-body matter with conditional generative adversarial networks,” *Phys. Rev. Res.* **4**, 033223 (2022).
- [37] Ye-Hua Liu and Evert P. L. van Nieuwenburg, “Discriminative cooperative networks for detecting phase transitions,” *Phys. Rev. Lett.* **120**, 176401 (2018).
- [38] Eliska Greplova, Agnes Valenti, Gregor Boschung, Frank Schäfer, Niels Lörch, and Sebastian D Huber, “Unsupervised identification of topological phase transitions using predictive models,” *New Journal of Physics* **22**, 045003 (2020).
- [39] Netta Karjalainen, Zina Lippo, Guangze Chen, Rouven Koch, Adolfo O. Fumega, and Jose L. Lado, “Hamiltonian inference from dynamical excitations in confined quantum magnets,” *Phys. Rev. Appl.* **20**, 024054 (2023).
- [40] Simone Tibaldi, Giuseppe Magnifico, Davide Vodola, and Elisa Ercolessi, “Unsupervised and supervised learning of interacting topological phases from single-particle correlation functions,” *SciPost Physics* **14**, 1–18 (2023), [arXiv:2202.09281](https://arxiv.org/abs/2202.09281).
- [41] Michael J. Hartmann and Giuseppe Carleo, “Neural-network approach to dissipative quantum many-body dynamics,” *Phys. Rev. Lett.* **122**, 250502 (2019).
- [42] Evert van Nieuwenburg, Eyal Bairey, and Gil Refael, “Learning phase transitions from dynamics,” *Phys. Rev. B* **98**, 060301 (2018).
- [43] Moritz Reh, Markus Schmitt, and Martin Gärttner, “Time-dependent variational principle for open quantum systems with artificial neural networks,” *Phys. Rev. Lett.* **127**, 230501 (2021).
- [44] Naeimeh Mohseni, Thomas Fösel, Lingzhen Guo, Carlos Navarrete-Benlloch, and Florian Marquardt, “Deep Learning of Quantum Many-Body Dynamics via Random Driving,” *Quantum* **6**, 714 (2022).
- [45] Giuseppe Carleo and Matthias Troyer, “Solving the quantum many-body problem with artificial neural networks,” *Science* **355**, 602–606 (2017).
- [46] Attila Szabo and Claudio Castelnovo, “Neural network wave functions and the sign problem,” *Phys. Rev. Res.* **2**, 033075 (2020).
- [47] Agnes Valenti, Eliska Greplova, Netanel H. Lindner, and Sebastian D. Huber, “Correlation-enhanced neural networks as interpretable variational quantum states,” *Phys. Rev. Res.* **4**, L012010 (2022).
- [48] Aldo Glielmo, Yannic Rath, Gabor Csanyi, Alessandro De Vita, and George H. Booth, “Gaussian process states: A data-driven representation of quantum many-body physics,” *Phys. Rev. X* **10**, 041026 (2020).
- [49] Moritz Reh, Markus Schmitt, and Martin Gärttner, “Optimizing design choices for neural quantum states,” *Phys. Rev. B* **107**, 195115 (2023).
- [50] Stefanie Czischek, Martin Gärttner, and Thomas Gasenzer, “Quenches near ising quantum criticality as a challenge for artificial neural networks,” *Phys. Rev. B* **98**, 024311 (2018).
- [51] I Rotter and J P Bird, “A review of progress in the physics of open quantum systems: theory and experiment,” *Reports on Progress in Physics* **78**, 114001 (2015).
- [52] J-W Zhang, J-Q Zhang, G-Y Ding, J-C Li, J-T Bu, B Wang, L-L Yan, S-L Su, L Chen, F Nori, *et al.*, “Dynamical control of quantum heat engines using exceptional points,” *Nature Communications* **13**, 6225 (2022).
- [53] Jan Perina Jr, Adam Miranowicz, Grzegorz Chimczak, and Anna Kowalewska-Kudlaszyk, “Quantum Liouvillian exceptional and diabolical points for bosonic fields with quadratic Hamiltonians: The Heisenberg-Langevin equation approach,” *Quantum* **6**, 883 (2022).
- [54] J.-T. Bu, J.-Q. Zhang, G.-Y. Ding, J.-C. Li, J.-W. Zhang, B. Wang, W.-Q. Ding, W.-F. Yuan, L. Chen, s. K. Ozdemir, F. Zhou, H. Jing, and M. Feng, “Enhancement of quantum heat engine by encircling a liouvillian exceptional point,” *Phys. Rev. Lett.* **130**, 110402 (2023).
- [55] Piotr Szankowski, “Introduction to the theory of open quantum systems,” *SciPost Phys. Lect. Notes* , 68 (2023).
- [56] Yuto Ashida, Zongping Gong, and Masahito Ueda, “Non-hermitian physics,” *Advances in Physics* **69**, 249–435 (2020).
- [57] Emil J. Bergholtz, Jan Carl Budich, and Flore K. Kunst, “Exceptional topology of non-hermitian systems,” *Rev. Mod. Phys.* **93**, 015005 (2021).
- [58] Nicola Maraviglia, Patrick Yard, Ross Wakefield, Jacques Carolan, Chris Sparrow, Levon Chakhmakhchyan, Chris Harrold, Toshikazu Hashimoto, Nobuyuki Matsuda, Andrew K. Harter, Yogesh N. Joglekar, and Anthony Laing, “Photonic quantum simulations of coupled \mathcal{PT} -symmetric hamiltonians,” *Phys. Rev. Res.* **4**, 013051 (2022).
- [59] Xiayu Linpeng, Léa Bresque, Maria Maffei, Andrew N. Jordan, Alexia Auffèves, and Kater W. Murch, “Energetic cost of measurements using quantum, coherent, and thermal light,” *Phys. Rev. Lett.* **128**, 220506 (2022).
- [60] Ayan Banerjee, Ronika Sarkar, Soumi Dey, and Awadhesh Narayan, “Non-hermitian topological phases: principles and prospects,” *Journal of Physics: Condensed Matter* **35**, 333001 (2023).
- [61] Wojciech Brzezicki, Matti Silveri, Marcin Plodzien, Francesco Massel, and Timo Hyart, “Non-hermitian topological quantum states in a reservoir-engineered transmon chain,” *Phys. Rev. B* **107**, 115146 (2023).
- [62] Yogesh N. Joglekar, Rahul Marathe, P. Durganandini, and Rajeev K. Pathak, “Pt spectroscopy of the rabi problem,” *Physical Review A* **90** (2014), 10.1103/physreva.90.040101.

- [63] Kaustubh S. Agarwal, Rajeev K. Pathak, and Yogesh N. Joglekar, “Exactly solvable PT-symmetric models in two dimensions,” *EPL (Europhysics Letters)* **112**, 31003 (2015).
- [64] Kaustubh S. Agarwal, Rajeev K. Pathak, and Yogesh N. Joglekar, “Raising the PT transition threshold by strong coupling to neutral chains,” *Physical Review A* **97** (2018), 10.1103/physreva.97.042107.
- [65] Zongping Gong, Yuto Ashida, Kohei Kawabata, Kazuaki Takasan, Sho Higashikawa, and Masahito Ueda, “Topological phases of non-hermitian systems,” *Phys. Rev. X* **8**, 031079 (2018).
- [66] Kohei Kawabata, Ken Shiozaki, Masahito Ueda, and Masatoshi Sato, “Symmetry and topology in non-hermitian physics,” *Phys. Rev. X* **9**, 041015 (2019).
- [67] Jiaming Li, Andrew K. Harter, Ji Liu, Leonardo de Melo, Yogesh N. Joglekar, and Le Luo, “Observation of parity-time symmetry breaking transitions in a dissipative floquet system of ultracold atoms,” *Nature Communications* **10** (2019), 10.1038/s41467-019-08596-1.
- [68] Tishuo Wang, Jianxiong Fang, Zhongyi Xie, Nenghao Dong, Yogesh N. Joglekar, Zixin Wang, Jiaming Li, and Le Luo, “Observation of two PT transitions in an electric circuit with balanced gain and loss,” *The European Physical Journal D* **74** (2020), 10.1140/epjd/e2020-10131-7.
- [69] Sharareh Sayyad, Jinlong Yu, Adolfo G. Grushin, and Lukas M. Sieberer, “Entanglement spectrum crossings reveal non-hermitian dynamical topology,” *Phys. Rev. Res.* **3**, 033022 (2021).
- [70] Weijian Chen, Maryam Abbasi, Yogesh N. Joglekar, and Kater W. Murch, “Quantum jumps in the non-hermitian dynamics of a superconducting qubit,” *Phys. Rev. Lett.* **127**, 140504 (2021).
- [71] Sharareh Sayyad and Flore K. Kunst, “Realizing exceptional points of any order in the presence of symmetry,” *Phys. Rev. Research* **4**, 023130 (2022).
- [72] Weijian Chen, Maryam Abbasi, Byung Ha, Serra Erdamar, Yogesh N. Joglekar, and Kater W. Murch, “Decoherence-induced exceptional points in a dissipative superconducting qubit,” *Phys. Rev. Lett.* **128**, 110402 (2022).
- [73] Maryam Abbasi, Weijian Chen, Mahdi Naghiloo, Yogesh N. Joglekar, and Kater W. Murch, “Topological quantum state control through exceptional-point proximity,” *Phys. Rev. Lett.* **128**, 160401 (2022).
- [74] Sharareh Sayyad, Marcus Stalhammar, Lukas Rodland, and Flore K Kunst, “Symmetry-protected exceptional and nodal points in non-hermitian systems,” [arXiv:2204.13945](https://arxiv.org/abs/2204.13945) (2022).
- [75] Kohei Kawabata and Masahito Ueda, “Nonlinear landauer formula: Nonlinear response theory of disordered and topological materials,” *Phys. Rev. B* **106**, 205104 (2022).
- [76] Sharareh Sayyad, “Protection of all nondefective twofold degeneracies by antiunitary symmetries in non-hermitian systems,” *Physical Review Research* **4**, 043213 (2022).
- [77] Zhenyu Xiao, Kohei Kawabata, Xunlong Luo, Tomi Ohtsuki, and Ryuichi Shindou, “Level statistics of real eigenvalues in non-hermitian systems,” *Phys. Rev. Res.* **4**, 043196 (2022).
- [78] Kohei Kawabata, Tokiro Numasawa, and Shinsei Ryu, “Entanglement phase transition induced by the non-hermitian skin effect,” *Phys. Rev. X* **13**, 021007 (2023).
- [79] Takahiro Fukui and Norio Kawakami, “Breakdown of the Mott insulator: Exact solution of an asymmetric Hubbard model,” *Physical Review B - Condensed Matter and Materials Physics* **58**, 16051–16056 (1998), [arXiv:9806023 \[cond-mat\]](https://arxiv.org/abs/9806023).
- [80] Berislav Buča, Cameron Booker, Marko Medenjak, and Dieter Jaksch, “Bethe ansatz approach for dissipation: exact solutions of quantum many-body dynamics under loss,” *New Journal of Physics* **22**, 123040 (2020).
- [81] Kazuki Yamamoto, Masaya Nakagawa, Kyosuke Adachi, Kazuaki Takasan, Masahito Ueda, and Norio Kawakami, “Theory of non-hermitian fermionic superfluidity with a complex-valued interaction,” *Phys. Rev. Lett.* **123**, 123601 (2019).
- [82] Masaya Nakagawa, Naoto Tsuji, Norio Kawakami, and Masahito Ueda, “Dynamical sign reversal of magnetic correlations in dissipative hubbard models,” *Phys. Rev. Lett.* **124**, 147203 (2020).
- [83] Masaya Nakagawa, Norio Kawakami, and Masahito Ueda, “Exact liouvillian spectrum of a one-dimensional dissipative hubbard model,” *Phys. Rev. Lett.* **126**, 110404 (2021).
- [84] X. Z. Zhang and Z. Song, “ η -pairing ground states in the non-hermitian hubbard model,” *Phys. Rev. B* **103**, 235153 (2021).
- [85] Timo Hyart and J. L. Lado, “Non-hermitian many-body topological excitations in interacting quantum dots,” *Phys. Rev. Res.* **4**, L012006 (2022).
- [86] Hironobu Yoshida and Hoshio Katsura, “Exact analysis of the Liouvillian gap and dynamics in the dissipative $SU(N)$ Fermi-Hubbard model,” [arXiv e-prints](https://arxiv.org/abs/2209.03743), 1–7 (2022), [arXiv:2209.03743](https://arxiv.org/abs/2209.03743).
- [87] Kazuki Yamamoto, Masaya Nakagawa, Masaki Tezuka, Masahito Ueda, and Norio Kawakami, “Universal properties of dissipative tomonaga-luttinger liquids: Case study of a non-hermitian xxz spin chain,” *Phys. Rev. B* **105**, 205125 (2022).
- [88] Ya-Nan Wang, Wen-Long You, and Gaoyong Sun, “Quantum criticality in interacting bosonic kitaev-hubbard models,” *Phys. Rev. A* **106**, 053315 (2022).
- [89] Ruizhe Shen and Ching Hua Lee, “Non-hermitian skin clusters from strong interactions,” *Communications Physics* **5**, 238 (2022).
- [90] Kazuki Yamamoto and Norio Kawakami, “Universal description of dissipative tomonaga-luttinger liquids with $SU(n)$ spin symmetry: Exact spectrum and critical exponents,” *Phys. Rev. B* **107**, 045110 (2023).
- [91] Sharareh Sayyad and Jose L. Lado, “Topological phase diagrams of exactly solvable non-hermitian interacting kitaev chains,” *Phys. Rev. Res.* **5**, L022046 (2023).
- [92] Ruizhe Shen, Tianqi Chen, Mohammad Mujahid Aliyu, Fang Qin, Yin Zhong, Huanqian Loh, and Ching Hua Lee, “Proposal for observing yang-lee criticality in rydberg atomic arrays,” *Phys. Rev. Lett.* **131**, 080403 (2023).
- [93] SangEun Han, Daniel J Schultz, and Yong Baek Kim, “Complex fixed points of the non-hermitian kondo model in a luttinger liquid,” [arXiv:2302.07883](https://arxiv.org/abs/2302.07883) (2023).
- [94] Sharareh Sayyad, “Non-hermitian chiral anomalies in interacting systems,” [arXiv:2306.14766](https://arxiv.org/abs/2306.14766) (2023), [arXiv:2306.14766](https://arxiv.org/abs/2306.14766).

- [95] Somsubhra Ghosh, K Sengupta, and Indranil Paul, “Hilbert space fragmentation imposed real spectrum of a non-hermitian system,” [arXiv:2307.05679](https://arxiv.org/abs/2307.05679) (2023).
- [96] Zhuo Cheng and Zhenhua Yu, “Supervised machine learning topological states of one-dimensional non-hermitian systems,” *Chinese Physics Letters* **38**, 070302 (2021).
- [97] Ling-Feng Zhang, Ling-Zhi Tang, Zhi-Hao Huang, Guo-Qing Zhang, Wei Huang, and Dan-Wei Zhang, “Machine learning topological invariants of non-hermitian systems,” *Phys. Rev. A* **103**, 012419 (2021).
- [98] Brajesh Narayan and Awadhesh Narayan, “Machine learning non-hermitian topological phases,” *Phys. Rev. B* **103**, 035413 (2021).
- [99] Waqas W Ahmed, Mohamed Farhat, Kestutis Staliunas, Xiangliang Zhang, and Ying Wu, “Machine learning for knowledge acquisition and accelerated inverse-design for non-hermitian systems,” *Communications Physics* **6**, 2 (2023).
- [100] Yefei Yu, Li-Wei Yu, Wengang Zhang, Huili Zhang, Xiaolong Ouyang, Yanqing Liu, Dong-Ling Deng, and L-M Duan, “Experimental unsupervised learning of non-hermitian knotted phases with solid-state spins,” *npj Quantum Information* **8**, 116 (2022).
- [101] Ce Shang, Shuo Liu, Ruiwen Shao, Peng Han, Xiaoning Zang, Xiangliang Zhang, Khaled Nabil Salama, Wenlong Gao, Ching Hua Lee, Ronny Thomale, *et al.*, “Experimental identification of the second-order non-hermitian skin effect with physics-graph-informed machine learning,” *Advanced Science* **9**, 2202922 (2022).
- [102] For computational purposes, the previous sum can be restricted to a subset of the lowest lying states.
- [103] We take $1/\lambda (= 0.005)$.
- [104] P Gersdorf, W John, J P Perdew, and P Ziesche, “Correlation entropy of the hsub 2 molecule,” *International Journal of Quantum Chemistry* **61** (1997), 10.1002/(SICI)1097-461X(1997)61:6;935::AID-QUA6j3.0.CO;2-X.
- [105] Z. Huang, H. Wang, and S. Kais, “Entanglement and electron correlation in quantum chemistry calculations,” *Journal of Modern Optics* **53**, 2543–2558 (2006).
- [106] Rodolfo O. Esquivel, Ana L. Rodriguez, Robin P. Sagar, Minhuy Ho, and Vedene H. Smith, “Physical interpretation of information entropy: Numerical evidence of the collins conjecture,” *Phys. Rev. A* **54**, 259–265 (1996).
- [107] Carlos L. Benavides-Riveros, Nektarios N. Lathiotakis, Christian Schilling, and Miguel A. L. Marques, “Relating correlation measures: The importance of the energy gap,” *Phys. Rev. A* **95**, 032507 (2017).
- [108] Per E. M. Siegbahn, Jan Almlöf, Anders Heiberg, and Björn O. Roos, “The complete active space SCF (CASSCF) method in a newton–raphson formulation with application to the HNO molecule,” *The Journal of Chemical Physics* **74**, 2384–2396 (1981).
- [109] Maxime Debortolis, Serge Florens, and Izak Snyman, “Few-body nature of kondo correlated ground states,” *Phys. Rev. B* **103**, 235166 (2021).
- [110] I. Snyman, “The structure of quasiparticles in a local Fermi liquid,” [arXiv e-prints](https://arxiv.org/abs/2308.15576), [arXiv:2308.15576](https://arxiv.org/abs/2308.15576) (2023), [arXiv:2308.15576](https://arxiv.org/abs/2308.15576) [cond-mat.str-el].
- [111] Tuomas I. Vanhala and Teemu Ojanen, “Complexity of fermionic states,” [arXiv e-prints](https://arxiv.org/abs/2306.07584), [arXiv:2306.07584](https://arxiv.org/abs/2306.07584) (2023), [arXiv:2306.07584](https://arxiv.org/abs/2306.07584) [quant-ph].
- [112] The Supplemental Material includes details on the architecture of neural networks, details on comparing predicted and true phase diagrams and further details on predicting non-Hemritian phase diagrams using non-Hemritian dataset.
- [113] Numerical calculations are performed using the dmrpgy package in <https://github.com/joselado/dmrgpy>.
- [114] Eric Jeckelmann, “Optical excitations in a one-dimensional mott insulator,” *Phys. Rev. B* **67**, 075106 (2003).
- [115] Li Ern Chern, Finn Lasse Buessen, and Yong Baek Kim, “Classical magnetic vortex liquid and large thermal hall conductivity in frustrated magnets with bond-dependent interactions,” *npj Quantum Materials* **6**, 33 (2021).
- [116] Diederik P Kingma and Jimmy Ba, “Adam: A method for stochastic optimization,” [arXiv:1412.6980](https://arxiv.org/abs/1412.6980) (2014).

Appendix A: Details on the architecture of neural networks

In the main text, we have presented the outcomes of our neural networks (NN). Here, we provide further details on how we build them up.

The architecture of our neural network (NN) consists of 1024/1024 hidden layers when the labels are $\mathcal{C}_{\text{corr}}$. When χ sets the labels, we consider either a regression problem with χ being treated as a real number or a classification problem with χ limited to discrete values of $\{1, 2, 4\}$ which are analytical orders of degeneracies in different phases. For the regression problem, the NN is built up using 128/1024/2048/1024/128 hidden layers while it has 128/1024/3072/1024/128 hidden layers when the classification problem is explored. The different numbers of hidden layers in NN architecture are attributed to the (dis)continuousness of $\mathcal{C}_{\text{corr}}(\chi)$. It is clear that the NN for the classification problem trains on more number of parameters. The final layer of the NN is a single dense layer to generate χ or $\mathcal{C}_{\text{corr}}$. For the classification problem, this last layer has a size of three associated with three classes of $\{1, 2, 4\}$.

Our NN models are optimized using the Adam algorithm [116] with a learning rate 10^{-6} . The loss function in the NN architecture is set to the mean absolute error unless for the classification problem where the categorical cross-entropy is chosen. The validation loss in the training steps is always less than 0.005. Except for the last layer, we used rectified linear unit (ReLU) as the activation function. The last layer for training data has the softmax activation function for the classification problem and is set to linear activation function in other cases.

Appendix B: Comparing predicted and true phase diagrams

To better understand the performance of the employed learning method, we compare the predicted and true phase diagrams. We note that the predicted phase diagram for the Hermitian model in Fig. 2 agrees quantitatively with the true phase diagram as shown in Fig. S1. This quantitative agreement between the predicted and true numerical results remains intact even when the non-Hermiticity is finite; see Sec. C. This suggests that the capability of NN in learning many-body effects is not limited to the realm of Hermitian physics.

We, however, note that the differences between true

and predicted phase diagrams of the non-Hermitian case, obtained using models on the Hermitian dataset display more features. Figure S2 (a) and (d) display the difference between the true (indicated by superscript t) and predicted phase diagrams using values of χ as the classifier. It is evident that a large portion of the phase diagram is incorrectly characterized where only two-point correlation functions are used to train the model; see panel (a). By employing both two-point and four-point correlation functions, the predicted phase diagram is significantly improved and merely small differences along the phase boundary and around $U = 0$ remain.

If we train the NN model using continuous values of χ as shown in panels (b) and (e), the predicted values using only two-point correlation functions are more accurate than in panel (a). Here, we again witness some discrepancy from the true results around $U = 0$, $U \approx \pm 2t$, or around $\eta = -1$. The results are slightly modified when four-point correlation functions are also used in training the NN model as inaccuracies around large values of U are eliminated.

When we employ $\mathcal{C}_{\text{corr}}$ instead of χ , the predicted results in the absence (c) or presence (f) of four-point correlation functions exhibit similar phase diagrams; although in difference is less pronounced in the absence of four-point correlation functions in panel (c). This might be rooted in the nature of the correlation entropy which is constructed from two-point correlation functions.

Appendix C: Predicting non-Hermitian phase diagrams using non-Hermitian dataset

In the main text, we present the prediction of non-Hermitian phase diagrams using NN models trained on Hermitian datasets. There, we have detected some discrepancies which we have attributed to the properties of non-Hermitian wavefunctions. Here, we present the prediction of non-Hermitian phase diagrams using NN models trained on the non-Hermitian datasets with $\delta = 0.5t$. Figure S3 displays the true (left column) and predicted (middle and left columns) phase diagrams. The NN models are trained using two-point correlation functions (middle column) or the combination of two-point and four-point correlation functions (right column). The employed labels for the data sets are the discrete values of χ (top row), the numerical values of χ (middle), and $\mathcal{C}_{\text{corr}}$ (bottom). In all panels, the phase diagrams are quantitatively reproduced, as the differences between the true (indicated by superscript t) and predicted values are very tiny as shown in Fig. S4.

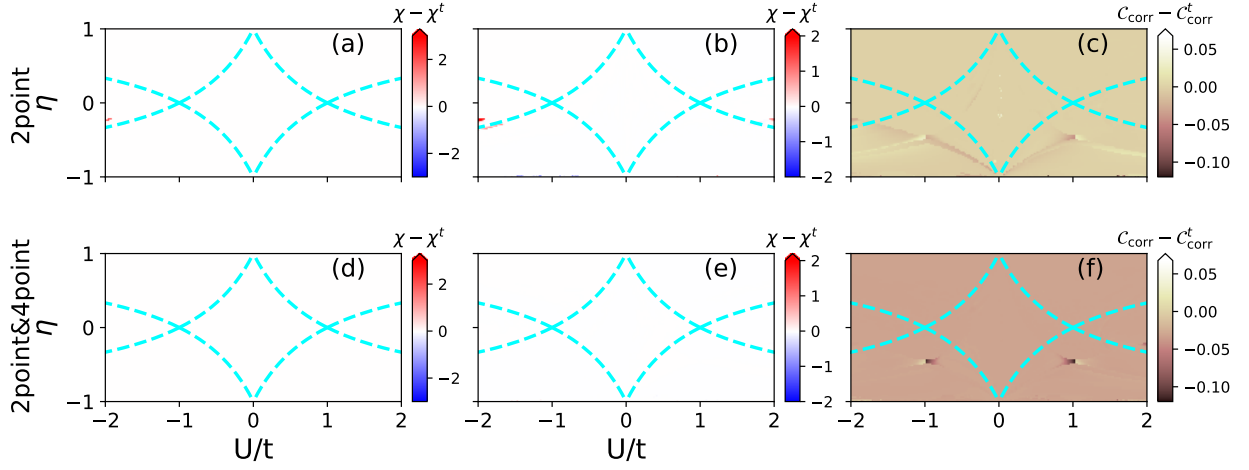


Figure S1. The difference between the predicted phase diagrams trained on the Hermitian dataset with the true Hermitian phase diagram at $\delta = 0.0$. The color bars denote the difference between the true (indicated by the superscript t) and predicted values of χ in panels (a), (b), (d), and (e) or C_{corr} in panels (c) and (f). The top panels are obtained for predicted phase diagrams using only two-point correlation functions shown in Fig. 2 (c) and (d). The bottom panels display the difference between the true and predicted values using both two-point and four-point correlation functions, shown in Fig. 2 (e), and (f).

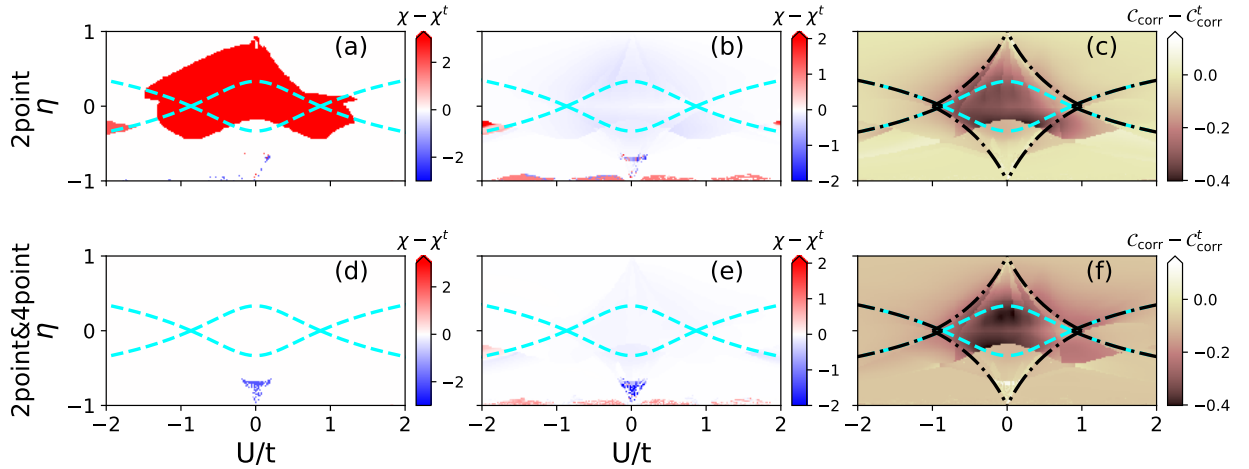


Figure S2. The difference between the predicted phase diagrams with $\delta = 0.5t$ trained on the Hermitian dataset with the true Hermitian phase diagram at $\delta = \delta_h = 0.0$. The color bars denote the difference between the true (indicated by the superscript t) and predicted values of χ in panels (a), (b), (d), and (e) or C_{corr} in panels (c) and (f). The top panels are obtained for predicted phase diagrams using only two-point correlation functions shown in Fig. 4 (b), (e), and (h). The bottom panels display the difference between the true and predicted values using both two-point and four-point correlation functions, shown in Fig. 4 (c), (f), and (i).

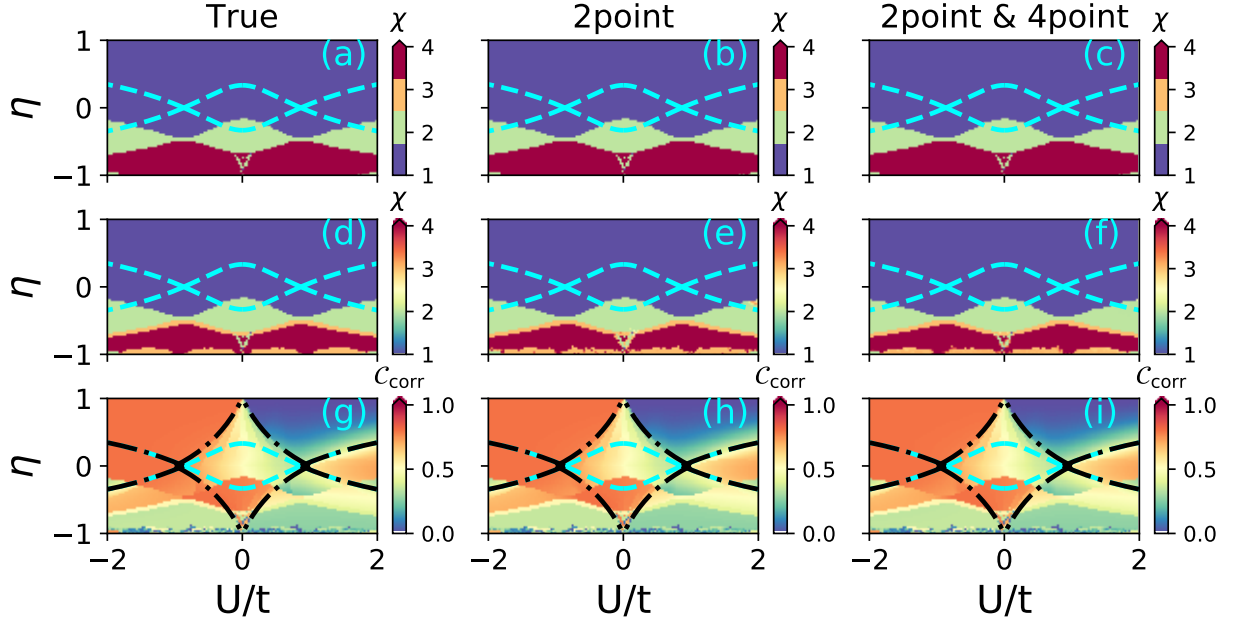


Figure S3. The phase diagram of the Kitaev-Hubbard chain with $L = 16$ on the $U/t - \eta$ plane at $\delta = 0.5t$. The color bar denotes χ (top and middle panels) and C_{corr} (bottom). The results in (a), (d), and (g) are calculated by exact diagonalization. The phase diagrams on the middle (right) column are obtained using the NN model trained by two-point (both two-point and four-point) correlation functions. $[\chi]$ in the top row is treated as a discrete classifier with $[\chi] \in \{1, 2, 4\}$ while it is treated as a continuous number in the panels of the middle row.

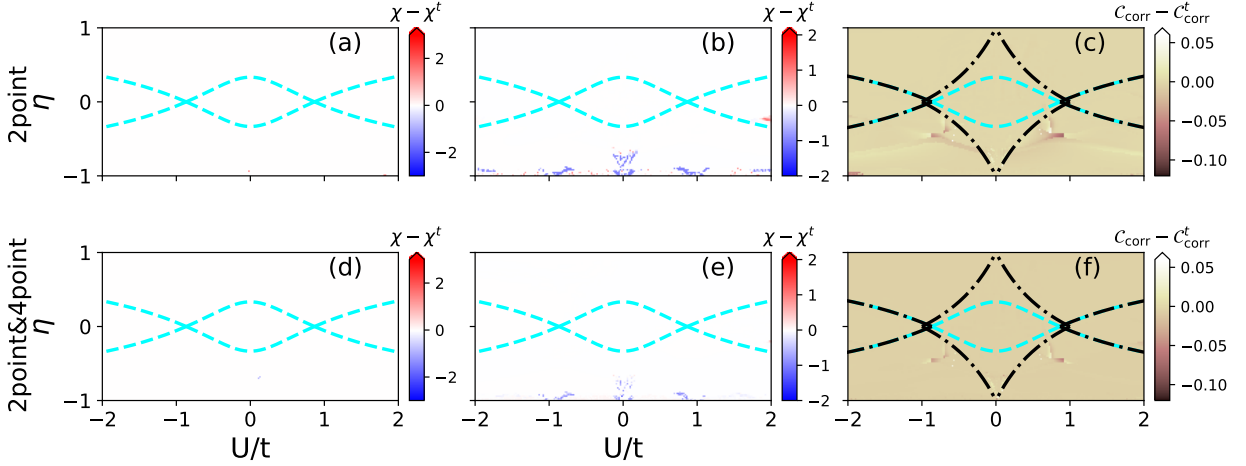


Figure S4. The difference between the predicted phase diagrams trained on the non-Hermitian dataset with the true non-Hermitian phase diagram at $\delta = 0.5t$. The color bars denote the difference between the true (indicated by the superscript t) and predicted values of χ in panels (a), (b), (d), and (e) or C_{corr} in panels (c) and (f). The top panels are obtained for predicted phase diagrams using only two-point correlation functions shown in Fig. S3 (b), (e), and (h). The bottom panels display the difference between the true and predicted values using both two-point and four-point correlation functions, shown in Fig. S3 (c), (f), and (i).